Turbulence characteristics of the I-mode confinement regime in ASDEX Upgrade

P. Manz[1,2], T. Happel[2], F. Ryter[2], M. Bernert[2], G. Birkenmeier[1,2], G.D. Conway[2], M. Dunne[2], L. Guimarais[3], P. Hennequin[3], A. Hetzenecker[1], C. Honoré[4], P. Lauber[2], M. Maraschek[2], V.E. Nikolaeva[3], D. Prisiazhniuk[2], U. Stroth[2,1], E. Viezzer[2,5] and the ASDEX Upgrade Team

[1] *Physik-Department E28, Technische Universität München, James-Franck-Str. 1, 85748 Garching, Germany*

[2] *Max-Planck-Institut für Plasmaphysik, Boltzmannstr.2 ,85748 Garching, Germany*

[3] *Instituto de Plasmas e Fusão Nuclear, Instituto Superior Técnico, Universidade Técnica de Lisboa, 1049-001 Lisboa, Portugal*

[4] *Laboratoire de Physique des Plasmas, Ecole Polytechnique, 91128 Palaiseau, France*

[5] *Department of Atomic, Molecular and Nuclear Physics, University of Seville, Avda. Reina Mercedes, 41012 Seville, Spain*

(Dated: May 18, 2017)

Turbulence in the I-mode confinement regime of ASDEX Upgrade exhibits beside strong geodesic acoustic mode (GAM) activity two prominent features, the weakly coherent mode (WCM) and strongly intermittent solitary density perturbations. The nonlinear interaction between these structures is studied in detail by means of a conditional averaged wavelet-bicoherence analysis. The wavelet analysis reveals that these density perturbations are at the WCM frequency. The GAM is coupled to all frequency scales of the velocity fluctuations via a modulational instability. The WCM shows coupling to higher frequencies prior to the bursts indicating a process resembling wave-steepening. A possible mechanism for the generation of such solitary density perturbations by a Korteweg-de-Vries-like nonlinearity is discussed.

PACS numbers:

I. INTRODUCTION

As large edge localized modes (ELMs) are a serious concern for reactors and even for ITER, intrinsically ELM-free regimes with good confinement as the I-mode would be an attractive operation regime for a fusion reactor. The I-mode is an improved confinement regime of tokamak plasmas operating in the unfavorable ion ∇B-drift direction combining H-mode-like energy confinement with L-mode-like particle and impurity transport [1]. It has been first described as the 'improved L-mode regime' on ASDEX Upgrade (AUG) [2], but the recent extensive studies in Alcator C-Mod [1, 3–7] have attracted attention as a possible operation scenario for ITER. An unharmful disadvantage is provided by the high L-I threshold compared to the L-H threshold in favorable ion ∇B-drift direction [8]. Furthermore, the I-mode in AUG [8] and DIII-D [9] often evolves slowly in an uncontrolled manner, until a transition to H-mode with large ELMs occurs. This would negate all advantages of the I-mode. It has been observed in both AUG and Alcator C-Mod that the power threshold from L- to I-mode scales at most weakly with the magnetic field ($P_{L-I} \sim B^{0.39}$ in AUG [10] and $P_{L-I} \sim B^{0.25}$ in C-Mod [7]) whereas the L- to H-mode power threshold scales nearly linear with B ($P_{L-H} \sim B^{0.8}$ [11]). This would enhance the operation window of the I-mode at higher magnetic fields compared to the small operation window faced in the majority of present day tokamak experiments. At a magnetic field of 8 T no transitions to H-mode have been observed in Alcator C-Mod [7]. This indicates that at high magnetic fields the I-mode may be a promising operation regime for a fusion reactor. To qualify the I-mode as an operating scenario for ITER, threshold and accessibility studies [8] also on a multi-machine basis [6] are needed.

In addition studies of turbulence in I-mode may offer a better understanding of the physics of the interaction of energy and particle transport barriers in general. The mechanism which selectively reduces only one of the transport channels is not understood. In the present contribution the turbulence characteristics of I-mode plasmas in AUG have been studied in detail. Two prominent features, the weakly coherent mode (WCM) [12] and the appearance of strongly intermittent density bursts [10, 13] as well as their connection are highlighted. Recent progress on confinement properties of I-mode plasmas in AUG will not be discussed in the present contribution, but can be found in Refs. [8, 10]. The new results presented in this manuscript include a detailed (conditional averaged bispectral) wavelet analysis to account for the strong intermittent behavior of turbulence in I-mode in AUG, a discussion of the kind of intermittency observed and a more detailed presentation of the suggestion for the generation of solitary waveforms by a Korteweg-de-Vries-like nonlinear, only shortly presented in the Letter [13], which is this time derived from the Braginskii equations.

II. FREQUENCY SPECTRA OF FLUCTUATIONS DURING I-MODE

Experiments were carried out on the ASDEX Upgrade tokamak (AUG), which has major and minor horizontal

radii of $R_0 = 1.65$ m and $a = 0.5$ m, respectively. The toroidal magnetic field strength was $B_0 = -2.5$ T and the plasma current was $I_p = 1$ MA. The presented discharges are in the upper-single null configuration, where the ion ∇B drift is directed away from the X-point providing the necessary high power threshold for H-mode access. The discharges discussed are representative of I-mode plasmas in AUG. Details on discharge parameters including background profiles can be found in [10, 12, 13].

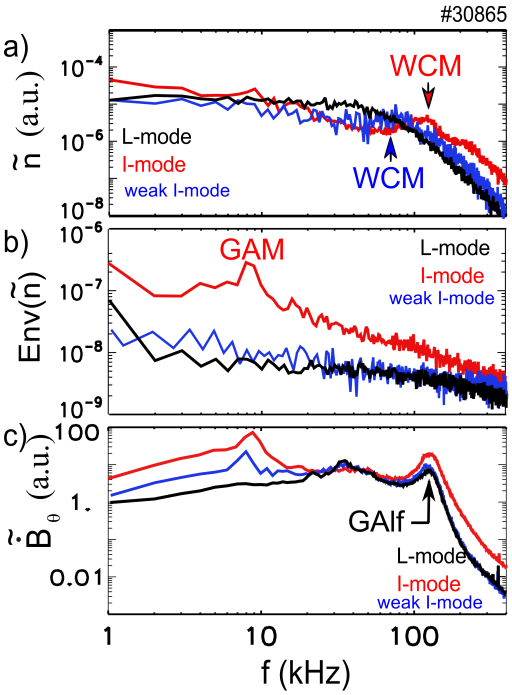

FIG. 1: (a) Spectrum of density fluctuations from frequency hopping reflectometry, (b) its envelope deduced from density fluctuations and (c) poloidal magnetic field fluctuations in L- (black) and I-mode (red). Also the spectra at the beginning of development of the I-mode (called weak I-mode) are shown in blue.

The density fluctuations shown in Fig. 1a are measured by hopping reflectometry diagnostic [14]. At the transition to I-mode the broadband region splits up into two bands in frequency space, one at low frequencies ($f < 30$ kHz) and one at higher frequencies ($80 < f < 150$ kHz). The band at higher frequencies is called the weakly coherent mode (WCM) [3]. This is the general characteristic fluctuation feature of the I-mode [3]. It is located in the steep gradient region at the very edge of the plasma [12]. In AUG the WCM appears at frequencies around 100 kHz with a width of a few 10 kHz (Fig. 1a) [12]. The wavenumber of the WCM in AUG is at $k_\theta \approx 1.5$ cm^{-1} [12] similar to the Alcator C-Mod results [5]. In addition to the WCM a geodesic acoustic mode (GAM) appears (Fig. 1b). Any flow as the GAM advects small-scale (high frequency) structures which leads to a modulation of perturbations at higher frequency. Therefore the effect of a flow can be approximated by the low frequency envelope of high frequency perturbations. This has been estimated by the envelope of density fluctuations above 400 kHz measured by hopping reflectometry as done in Ref. [15] and described in detail in Ref. [12, 16]. The GAM advects the WCM and leads to the broadening through the Doppler effect [12], this constitutes the energy transfer as seen in Ref. [5]. The basic instability of the WCM is still unknown, recent simulations with BOUT++ indicate a simple drift-Alfénic instability [17].

In AUG magnetic fluctuations close to the WCM are amplified during the I-mode (Fig. 1c). Using the measured background profiles the gyrokinetic eigenvalue solver LIGKA [18] is used to determine the kinetic continuum branches of toroidal symmetric modes. Two modes, the GAM ($m = 0$, $f \sim 10$ kHz) and a global Alfénic mode ($m = 1$, $f \sim 140$ kHz) called the geodesic Alfénic mode (GAlf) are close to the experimentally observed frequencies. The GAlf is similar to the mode previously observed in TFTR [19]. The frequency of the magnetic fluctuations close to the WCM frequency coincides with the GAlf frequency [12]. Comparisons with the Mirnov coils show the characteristic toroidal and poloidal mode numbers of the GAlf of zero and one, respectively [12]. However, these magnetic fluctuations are already present in L-mode (Fig. 1c). As seen in the early weak I-mode (blue line in Fig. 1), where the pressure gradients just slightly steepen up and the confinement just increases slightly at constant heating power [12], the frequency of the WCM ($f_{WCM} \sim 70$ kHz, blue line in Fig. 1a) is smaller compared to the developed I-mode ($f_{WCM} \sim 130$ kHz, red line in Fig. 1a). The magnetic fluctuations (GAlf) do not change ($f_{GAlf} \sim 140$ kHz, Fig. 1c) and WCM and GAlf do not coincide in frequency in the weak I-mode case. Therefore, it should be stressed WCM and GAlf are not the same mode.

III. STRONGLY INTERMITTENT DENSITY FLUCTUATIONS

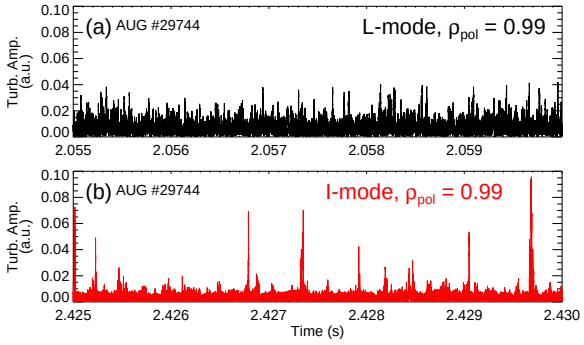

FIG. 2: Comparison of turbulence amplitude behavior in (a) L- and (b) I-mode measured with Doppler reflectometry.

The edge turbulence in L-mode is characterized by

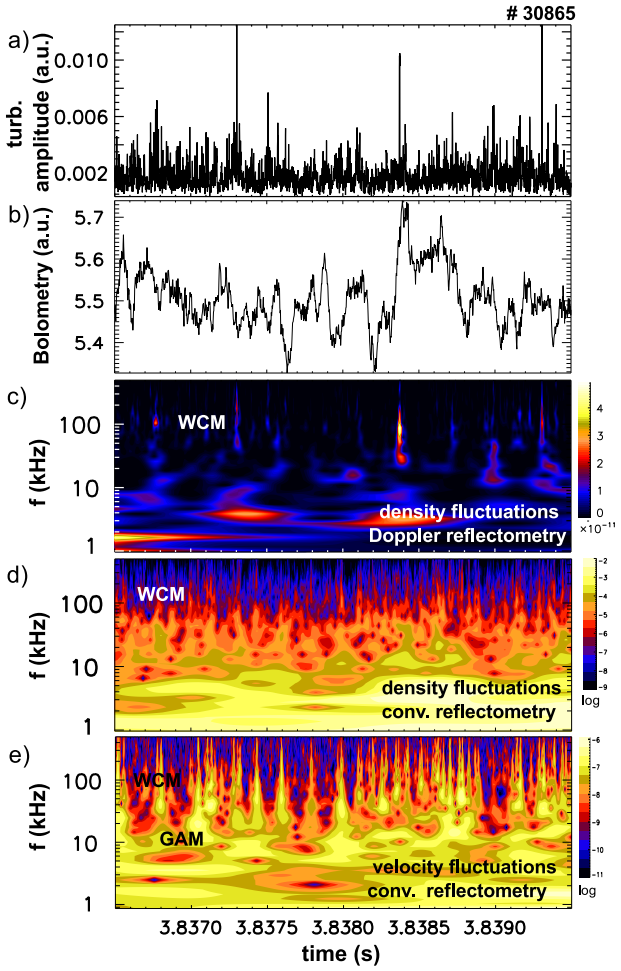

FIG. 3: Turbulent amplitude of density fluctuations measured by Doppler reflectometry (a), radiative fluctuations at the upper divertor measured by AXUV bolometry (b), wavelet transform of these density fluctuations (c), of density fluctuations measured by conventional reflectometry (d) and of the envelope fluctuations as a proxy for velocity fluctuations measred by the conventional reflectometry (e).

broadband fluctuations as measured by Doppler reflectometry (DR) in Fig. 2a. While the background density turbulence level is reduced in I-mode compared to the L-mode level, the I-mode in AUG exhibits strong intermittent density bursts (Fig. 2b) causing a heavy-tail probability distribution function [10, 13]. The bursts exhibit a solitary waveform and last for about 2–10 μs [10, 13]. These bursts are not ELMs, the peeling-ballooning stability boundaries are far away from the experimental parameters in I-mode as calculated with the MISHKA code [10]. Furthermore, no pronounced magnetic signature as typical for type-I ELMs [20] is observed.

Turbulence bursts also occur in the late I-phase [21]. However, the bursts in I-phase appear more regular in time with a much longer duration. Also the bursts exhibit type-III ELM-like precursors in the late I-phase [22] which is usually not observed in I-mode. The bursts in I-mode show some similarities to inter-ELM fluctuations in H-mode as previously observed [23]. A detailed study on this similarity is left for future work.

Most importantly, the intermittent events show up in the divertor measured by absolute extended ultraviolet (AXUV) diode based bolometry [24] several tens of microseconds later than observed with the DR in the confined region at the minimum of the radial electric field [10]. The radiative response in the divertor is much longer in time than the bursts measured with the DR [10]. The divertor impact in combination with the strong density perturbation in the confined region suggests that these bursts are playing an important role in hampering the density pedestal to develop although a proof by direct measurements of the particle transport is not possible as the bolometer measurement is a combination of density, temperature, and impurity concentration.

Previous results show a strong correlation between density bursts and the WCM [13]. Complementary to the previous analysis [13], a wavelet-based approach is used here. For strongly intermittent time series containing short-lived events a wavelet analysis avoids averaging out temporally localized events compared to a Fourier-based analysis. The wavelet transform is given by

$$\tilde{n}(t) \rightarrow \tilde{n}(f,t) = \int d\acute{t}\psi(t-\acute{t})\tilde{n}(\acute{t}) \qquad (1)$$

where the complex Morlet wavelet $\psi(t) = C(e^{i2\pi t} - e^{-2\pi^2})e^{-t^2/2}$ is used here, where C is a real constant. Figure 3a shows the amplitude of density fluctuations in I-mode measured by the Doppler reflectometry as a reference. (the square root of the squared I and Q signal is used). In Fig. 3b radiative fluctuations measured by the AXUV bolometry at a line of sight measuring just outside the confined region in the upper divertor (DVC48) are shown. A general correlation is not that obvious. However, the strongest activity of the WCM at around $t = 3.9384$ s is accompanied by a clear radiative response in the upper divertor. Closer to the I-H transition the correlation between bursts and radiative fluctuations in the upper divertor is more evident as shown in Ref. [10]. The wavelet transform of the density fluctuations measured by DR are shown in Fig. 3c. The density bursts are perturbations at the WCM frequency at around 100 kHz. The wavelet analysis of the phase measured by conventional reflectometry shows also an intermittent activity of the WCM (Fig. 3d). Strong activity of global modes (as the GAM or WCM) can lead to strongly localized turbulent activity. Due to turbulence localization the transport can become bursty [25]. The envelope of the phase fluctuations measured by the conventional reflectometry which is a measure of the velocity fluctuations is investigated. The envelope is estimated from the high pass filtered (above 400 kHz) phase fluctuations. Also the envelope which can be seen as an approximation for the flow is fluctuating intermittent showing features at the GAM and WCM frequency (Fig. 3e).

An intermittent behavior of the GAM is not unusual and has been reported from most devices [26–38]. Intermittent transport associated with the GAM has been studied theoretically near the critical gradient regime [39]. Where the GAMs emit turbulence energy in bursts, the energy of stationary zonal flows can accumulate gradually due to the undamped residues. This leads to a dynamical increase in turbulence quenching as well as to a nonlinear upshift of the critical gradient (i.e. the Dimits shift) [39]. This might be related to the observed spontaneous uncontrolled non-steady improvement of confinement of the I-mode which most often leads to a transition to H-mode [8].

IV. ON EXTERNAL AND INTERNAL INTERMITTENCY

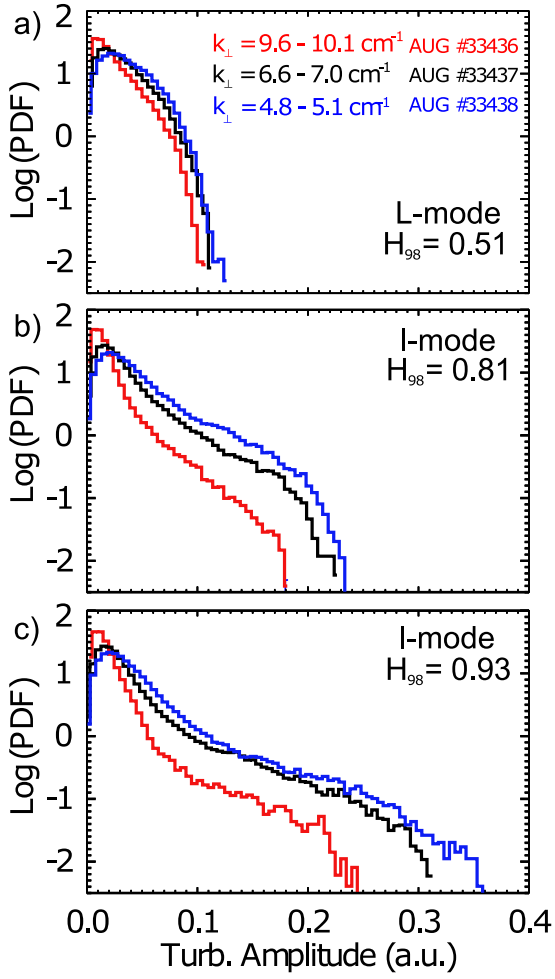

FIG. 4: PDFs of density fluctuation amplitudes obtained at $\rho_{pol} = 0.99$ for different sizes, $k_\perp \approx 10$ cm^{-1}, $k_\perp \approx 7$ cm^{-1}, $k_\perp \approx 5$ cm^{-1} shown at the same level of confinement in L-mode ($H_{98} = 0.51$) (a) and I-mode ($H_{98} = 0.81$ (b) and $H_{98} = 0.93$ (c)). Heavy tails develop with improved confinement in I-mode. Larger structures show more pronounced tails.

The term intermittency describes two distinct aspects of turbulent flows [40]. These are not independent. The first one, the so-called external intermittency, is associated with partly-turbulent flows, with the strongly irregular and convoluted structure and random appearance of turbulent and nonturbulent fluid [40]. External intermittency is characterized by an on-off variation. This on-off variation induces the strong deviation from Gaussian statistics [40]. This kind of intermittency is a key problem for renewable energy as solar generators only produce energy when the sun is shining or wind mills only produce energy as the wind is blowing. Also intermittency in the context of critical phenomena as in stock market dynamics or earth quakes for example is related to this kind of intermittency and is not related to a particular scale as the on-off variation effects all scales. The second aspect is the so-called internal or small-scale intermittency, which is usually associated with the tendency to spatial and temporal localization of the fine- or small-scale structure of flows always in the turbulent state [40]. This kind of intermittency is related to dissipation at the smallest scales and possibly to a deviation from self-similarity in the large wavenumber region.

The perpendicular wavenumber measured with the Doppler reflectometer has been scanned between $k_\perp \approx 5$–10 cm^{-1}. The deviation from Gaussian statistics increases with improving confinement [10, 13] as seen in Fig. 4 by the probability distribution function (PDF) of the density fluctuation amplitude. The density bursts are not only observed when small structures are probed, but also at rather large scales. At large scales the development of the heavy tail in the PDF is even more pronounced. Therefore, the intermittency in I-mode seems not to be related to small-scale intermittency in particular, but first of all to external intermittency.

External intermittency is a basic process of the transition from a laminar to a turbulent flow. At the transition from laminar to turbulent flows, laminar and turbulent regions coexist in the same flow. The Kármán vortex street is a well known example for this. This is consistent with the kind of intermittency observed by DR in I-mode. The turbulence is most of the time strongly suppressed and the fluctuations are restricted to small periods in time. Interestingly there is a further similarity with a specific transition scenario to a turbulent state. The transition to drift-wave turbulence is found to follow the Ruelle-Takens scenario [41]. By increasing the control parameter the system passes through different regimes from periodic to quasi-periodic to mode locked to weakly turbulent. In the mode locked regime a quasi-coherent mode appears [42]. In this regime a large-scale flow structure is generated by the inverse energy cascade process and coupled to small-scale density fluctuations [43]. Through this coupling the density perturbations are phase locked and synchronized to the large-scale flow and appear as a quasi-coherent mode [43]. This appears to be similar to the WCM, where the density fluctuations are phase locked by the GAM [12]. From this point of

view, the I-mode can be seen to be at the transition to turbulence. Also other high confinement regimes exhibit quasi coherent modes and may be considered to be rather at the transition to turbulence than turbulent. For example in the usual H-mode also quasi-coherent fluctuations appear in the magnetics at high frequency [44, 45] and the turbulence level is small.

V. NONLINEAR INTERACTION BETWEEN GAM, WCM AND DENSITY BURSTS

To investigate the nonlinear coupling between GAM, WCM and the density bursts, the conditional averaged wavelet-bicoherence [46] is estimated. It is based on three existing techniques, the wavelet analysis, the bispectral analysis and conditional averaging. Bispectral analysis is used to investigate the nonlinear interaction between different frequencies. Nonlinear interactions take place in frequency and as well in wavenumber space and has to fulfill the three-wave-coupling condition in both frequency $f = f_1 + f_2$ and in wavenumber space $k = k_1 + k_2$. The Doppler reflectometer is sensitive only to one wavenumber and the three-wave-coupling condition in wavenumber space cannot be fulfilled. For this reason the conventional reflectometer is used for the following bispectral analysis. The wavelet analysis is needed to investigate short-lived events like the density bursts in I-mode and the conditional average provides the possibility to focus on these events. The density fluctuations (approximated by the circular phase signal as described above) is divided in overlapping subwindows of 1200 μs length and the wavelet transform is performed with a lowest frequency of 2.5 kHz. To avoid boundary effects only the central part with a length of 400 μs is used for the following analysis. Via advection by the flow $v_\perp$, the density $\tilde{n}$ is subject to a nonlinearity $\tilde{v}_\perp \nabla_\perp \tilde{n}$ which can be studied by means of the cross-bicoherence of density fluctuations $\tilde{n}(f_1)$ and the envelope $\mathrm{Env}(f_2)$ representing the flow

$$\hat{b}^2_{nnE}(f_1, f_2, t) = \frac{\left|\langle \tilde{n}(f_1,t)\mathrm{Env}(f_2,t)\tilde{n}^*(f_1+f_2,t)\rangle\right|^2}{\langle|\tilde{n}(f_1,t)|\rangle^2\langle|\mathrm{Env}(f_2,t)|\rangle^2\langle|\tilde{n}(f_1+f_2,t)|\rangle^2}. \quad (2)$$

Using the more direct measurement of the velocity provided by DR instead seems tempting, but density and velocity have to be measured at the same position. This cross-bicoherence gives the degree of phase locking between the three different modes $\tilde{n}(f_1)$, $\mathrm{Env}(f_2)$ and $\tilde{n}(f_1 + f_2)$ and takes values between zero and one. Phase locking is a necessary condition for nonlinear coupling. As a trigger for the conditional average the density fluctuations have been bandpass filtered between 100 and 200 kHz to estimate the WCM activity. Fluctuating data of 250 ms (3.75–4.0 s) is conditional averaged over 119 events (indicated by the brackets $\langle\cdot\rangle$) exceeding the standard deviation of the trigger signal by a factor of 2.5 at the rising edge of the bandpass-filtered (100-200 kHz) density perturbations. The corresponding significance level is about 0.01. The conditional averaged WCM density burst is shown in Fig. 5a (with the black line) together with the wavelet power spectrum of the not bandpass filtered density perturbations also conditional averaged with the same condition. An increase in the WCM amplitude is observed. Compared to the envelope fluctuations it is observed that the WCM fluctuations in the density (Fig. 5a) are accompanied by velocity fluctuations (Fig. 6a).

In the following, the general coupling features are described. In I-mode a pronounced coupling of the center of gravity proportional to velocity fluctuations at low frequency of the GAM-like mode ($\sim$ 10 kHz) with the WCM (70–140 kHz) is found (see (A) in Figs. 5b–d) as reported previously [12]. The velocity fluctuations of the WCM ($f_2 = \pm f_{WCM}$) are coupled to fluctuations near the WCM frequency ($f_1 = f_{WCM}$) and the second harmonics of the WCM band (f_1 = 140–280 kHz) (see (B) in Figs. 5b–c). The coupling between the GAM-like mode and WCM can be also observed in the auto-bicoherence of the envelope fluctuations

$$\hat{b}^2_{EEE}(f_1, f_2, t) = \frac{\left|\langle \mathrm{Env}(f_1,t)\mathrm{Env}(f_2,t)\mathrm{Env}^*(f_1+f_2,t)\rangle\right|^2}{\langle|\mathrm{Env}(f_1,t)|\rangle^2\langle|\mathrm{Env}(f_2,t)|\rangle^2\langle|\mathrm{Env}(f_1+f_2,t)|\rangle^2}. \quad (3)$$

This resembles the effects of the nonlinearity $\tilde{v}_\perp \nabla_\perp \tilde{v}_\perp$ in the polarization equation, responsible for the inverse energy cascade and structure formation including the Reynolds stress. In general, the GAM frequency is coupled to all other frequencies indicating the modulation instability [47, 48] which is equivalent to the Reynolds stress drive of the GAM. Here, the GAM is primarily coupled to the WCM (see (A) in Figs. 6b–d) and once higher frequencies are excited, these are also coupled to the GAM as indicated by the extension of the lines in the center.

Next, the time dependence of the nonlinear coupling process is described. At $\tau = -20$ μs the velocity fluctuations of the WCM are coupled to higher frequencies $f_1 > 140$ kHz in the density (see (B) in Fig. 5b). This coupling increases with time. At $\tau = -10$ μs velocity fluctuations at the WCM frequency $f = f_{WCM}$ are coupled to themselves generating higher harmonics (see (C) in Fig. 6b). The induced high frequency velocity fluctuations can now modulate the density, leading to perturbations at higher frequencies in the density (see (D) in Fig. 5c) as well in the velocity (see (E) in Fig. 6c). Like in a self steepening process higher and higher frequencies are getting involved in the generation of the burst.

One of the main reasons for small-scale intermittency is thought to be the direct interaction (or non-local coupling) of large and small scales [40, 49]. Small-scale intermittency spends a very short time at very small scales. The power and the amplitudes at high wavenumbers (small scales) and short times (high frequencies) is

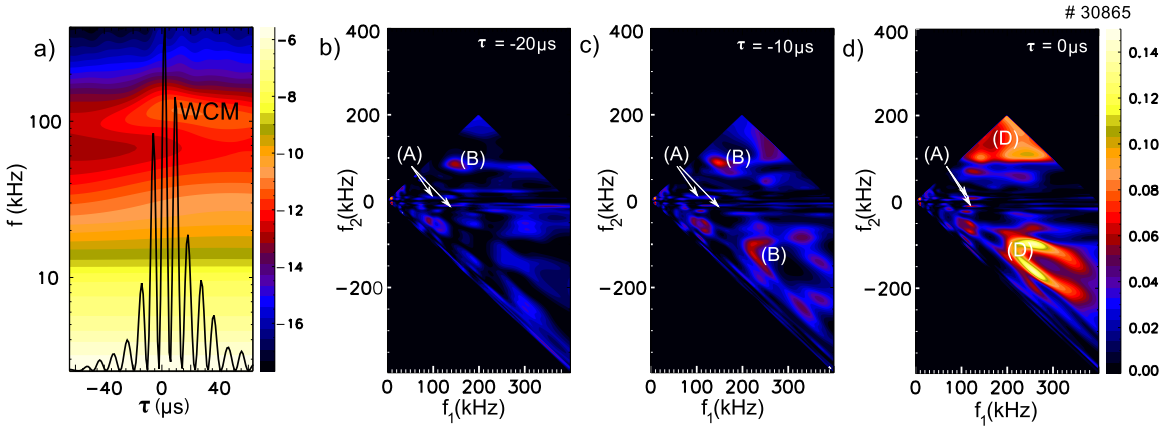

FIG. 5: Conditional averaged density burst (black, a), conditional averaged wavelet powerspectrum of density fluctuations (a), the conditional averaged cross-bicoherence $\hat{b}^2_{nnE}(f_1, f_2, \tau)$ at $\tau = -20$ μs (b), $\tau = -10$ μs (c) and $\tau = 0$ μs (d) with respect to the conditional averaged WCM density burst.

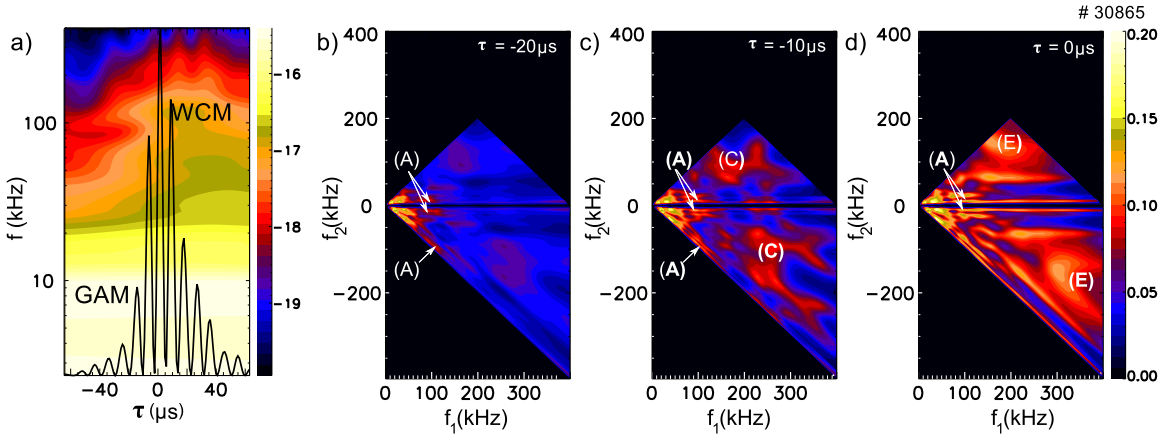

FIG. 6: Conditional averaged WCM density burst (black, a as in Fig. 5a), conditional average of the wavelet powerspectrum of the envelope fluctuations (a), the conditional averaged auto-bicoherence $\hat{b}^2_{EEE}(f_1, f_2, \tau)$ at $\tau = -20$ μs (b), $\tau = -10$ μs (c) and $\tau = 0$ μs (d) with respect to the conditional averaged WCM density burst.

small. To be intermittent the power, which is at the large scales has to be transmitted to the small scales in a very short time. Non-local coupling in wavenumber space provides such a possibility. Even though the intermittency in I-mode is of the kind of external intermittency, the energy has to be transmitted from low to high frequencies also in this case. A non-local coupling between large and small scales is observed here by the coupling of the GAM-like mode at large scales with the WCM at smaller scales and even smaller scales of the bursts and might be the reason for the intermittency. It should be noted that only the possibility of energy transfer and not the net energy transfer is measured by the bicoherence. If the basic instability of the WCM grows, it is suppressed by the Reynolds stress (see (A) in Figs. 6b–d). This suppression occurs due to transfer of kinetic energy from the WCM and all other modes to the GAM. The energy transfer is proportional to the flow shear [50], which is higher for higher confinement.

VI. GENERATION OF SOLITARY-LIKE STRUCTURES

The density bursts exhibit a solitary waveform. Solitons are a result of a competition between self-steepening by a nonlinearity and dispersion as described for example in 1D by the Korteweg-de-Vries (KdV) equation. The non-linearity appearing in the KdV and Burgers equations are known to be responsible for intermittency in 1D systems [51]. Self-steepening results in the generation of higher harmonics. This is not possible for the standard nonlinearity in a magnetized plasma given by the advection by the $E \times B$ drift $v_{E\times B} \cdot \nabla_\perp = \frac{\mathbf{B}\times\nabla_\perp\tilde{\phi}}{B^2}\nabla_\perp$,

with magnetic field $\mathbf{B} = B\hat{\mathbf{z}}$ in $\hat{\mathbf{z}}$ direction and strength B and electrostatic potential $\tilde{\phi}$. It can be written as $\frac{T_e}{eB\rho_s^2}(\hat{\mathbf{z}}\times\nabla_\perp\tilde{\phi})\cdot\nabla_\perp$ with electron temperature T_e, elementary charge e and $\rho_s = \sqrt{T_e m_i}/eB$. In wavenumber space $\nabla_\perp \to i\mathbf{k}$ this is proportional to $(\hat{\mathbf{z}}\times\mathbf{k})\cdot\mathbf{k}' = \hat{\mathbf{z}}(\mathbf{k}'\times\mathbf{k})$. Therefore higher harmonics $\mathbf{k}' = c\mathbf{k}$ with constant scalar c cannot be generated directly. The observation of the generation of higher harmonics in the bispectrum ((B) in Fig. 5) is not as trivial as it seems.

Here, one possibility for the generation of such solitary-like structures is shown. Starting point is the advective part of the electron temperature of the Braginskii equation [52]

$$\frac{3}{2}n\frac{dT_e}{dt} = \frac{3}{2}\left(n\frac{\partial T_e}{\partial t} + nv_{E\times B}\nabla_\perp T_e\right). \tag{4}$$

In the next step, temperature and density are divided by typical values, n_0 and T_{e0}, respectively. The normalized density and temperature are decomposed in background and fluctuating quantities $n = \bar{n} + \tilde{n}$ and $T_e = \bar{T}_e + \tilde{T}_e$. Making use of the Poisson bracket $v_{E\times B}\nabla_\perp = \left\{\tilde{\phi},\cdot\right\} = \partial_x\tilde{\phi}\partial_y - \partial_y\tilde{\phi}\partial_x$, with x the radial and y the binormal coordinate, the advective part can be written as

$$\frac{\partial\tilde{T}_e}{\partial t} = \bar{n}\left\{\tilde{\phi},\tilde{T}_e\right\} + \tilde{n}\left\{\tilde{\phi},\bar{T}_e\right\} + \tilde{n}\left\{\tilde{\phi},\tilde{T}_e\right\} \tag{5}$$

In drift-wave ordering the gradients of the fluctuations are in the order of the gradients of the background values, therefore the first term is the highest in drift-wave ordering and the last two terms would be neglected. As a product of three fluctuating quantities the third term is negligibly small. However, the second term can be written as

$$\frac{\partial\tilde{T}_e}{\partial t} \sim \tilde{n}\frac{\partial\tilde{\phi}}{\partial y}\frac{\partial\bar{T}_e}{\partial x} \tag{6}$$

and in the case of these strong density bursts in I-mode, the density fluctuation level as well as the background temperature gradient are considered to be high. On the other hand the first term in competition is proportional to the temperature fluctuation level, which is considered to be low. This has been observed to be the case in Alcator C-Mod [53]. A confirmation in AUG is still pending. The transition of the dominant turbulence regime from drift-wave dominated to resistive ballooning dominated is expected to occur at $C\omega_B > 1$ [54], where the local normalized collisionality is given by $C = 0.51(m_e/m_i)(qR/L_\perp)^2\nu_e(L_\perp/c_s)$ and $\omega_B = 2L_\perp/R$ with electron and ion masses m_e and m_i, respectively, safety factor q, collisionality ν_e and ion sound speed $c_s = \sqrt{T_e/m_i}$. For $n_e = 2.5\cdot10^{19}$ m^{-3}, $T_e = 250$ eV, $q = 5$ and $L_\perp = 2.5$ cm at $\rho = 0.98$ we get $C \approx 1$ and $\omega_B \approx 7.5\cdot10^{-3}$ hence $C\omega_B \ll 1$. It seems reasonable at these low collisionalities at high temperatures to assume adiabatic electrons with $\tilde{\phi} \approx \tilde{n}$. In this case the nonlinearity has the form $\sim \tilde{n}\partial_y\tilde{n}$ of a KdV-nonlinearity explicitly proportional to the radial temperature gradient. Therefore, drift-wave turbulence with intrinsically low transport can generate solitary-like temperature perturbations. How are those transmitted to the density? The adiabatic coupling including temperature perturbations is given by $\tilde{h} = \tilde{\phi} - \tilde{n} - 1.71\tilde{T}_e \approx 0$ [52]. The temperature fluctuations can be approximated by $\tilde{T}_e \approx (\tilde{\phi} - \tilde{n})/1.71$. For low temperature fluctuations $\tilde{\phi} \approx \tilde{n}$ is still valid. Therefore there is no contradiction with the argumentation above. Defining a small phase difference δ between potential and density fluctuations with $\tilde{\phi} = \tilde{n}(1 - i\delta)$, it follows $\tilde{T}_e \approx (\tilde{\phi} - \tilde{n})/1.71 = \tilde{n}(1 - 1 - i\delta)/1.71$. Density fluctuations can be induced by the temperature fluctuations as $\tilde{n} \approx (i1.71\tilde{T}_e)/\delta$. If the phase difference δ is small the bursts appear larger in the density than in the temperature. The temperature fluctuations also lead to particle transport $\Gamma = \tilde{v}_{E\times Bx}\tilde{n} = i(k_y/B)\tilde{\phi}\tilde{n}$. With the $i\delta$ response this can be written as $\Gamma = -(k_y/B)\delta\tilde{n}^2 = +(k_y 1.71^2\tilde{T}_e^{\,2})/(\delta B)$. The associated heat transport is $q = \tilde{v}_{E\times Bx}\tilde{n}\tilde{T}_e = -(k_y 1.71^2\tilde{T}_e^3/(\delta B)$ which is small as $\tilde{T}_e$ is small and in the other direction as the particle transport.

One possible scenario for the generation of solitary-like density perturbations regulating the particle transport is the following: a close to adiabatic coupling between potential and density can induce a solitary-like perturbation in the electron temperature, if the density fluctuation level and the electron temperature gradient are high and the electron temperature fluctuation level is low. This temperature perturbation can be proportional to the phase shift between potential and density and an increase of the temperature fluctuation level can lead to an increase in particle transport accompanied by a soliton-like waveform in the density induced by the adiabatic coupling. By means of line ratio spectroscopy on helium [55] or correlation electron cyclotron emission [56] it may be possible in the near future in AUG to measure density and temperature fluctuations at the same point in space and time and hence their cross-phase allowing a quantitative examination of the presented scenario.

VII. SUMMARY

Recent studies of I-mode turbulence in ASDEX Upgrade have shown two prominent features, the weakly coherent mode [12] and strongly intermittent density bursts [13]. The divertor impact in combination with the strong density perturbation in the confined region suggests that these bursts are playing an important role in hampering the density pedestal to develop [10]. As indicated in [10] and shown by the wavelet analysis here (Fig. 3) both features are strongly coupled. In ASDEX Upgrade the short-lived (2–10 μs) intermittent density fluctuations measured by Doppler reflectometry (at $k_\perp$ = 5–13 cm^{-1}) appear at the WCM frequency. The WCM measured by the conventional reflectometry (at smaller $k_\perp$ = 0–2 cm^{-1}) shows also an intermittent behavior.

A strong activity of global modes (the GAM in the I-mode case) leads to strongly localized turbulent activity. Heavy tails in the probability distribution function of the density fluctuation amplitudes are more pronounced at larger scales. Together with the on-off variation of the fluctuations the intermittency in I-mode seems to be of the kind of external intermittency at the transition to turbulence in a phase-locked regime. Due to high turbulent amplitudes, nonlinear processes are getting more important and the transport can become bursty [25]. The WCM in density measured by conventional reflectometry is accompanied by fluctuations in the envelope of high frequency fluctuations at the WCM frequency. The envelope fluctuations can be interpreted as flow perturbations at the WCM frequency. These fluctuations also modulate density and velocity fluctuations at even higher frequencies. The nonlinear behavior during strong WCM activity shows an increase in high frequency activity similar to a wave-steepening process. A Korteweg-de-Vries-like nonlinearity could be responsible for the intermittent behavior and the solitary waveforms as observed in the experiment [13]. The explicit temperature gradient dependence of this nonlinearity may explain why the bursts are that pronounced in I-mode [13]. This nonlinearity also provides a possibility to selectively reduce only one of the transport channels. However, this possibility awaits verification until combined fast temperature and density measurements are available.

Acknowledgements

This work has been carried out within the framework of the EUROfusion Consortium and has received funding from the Euratom research and training programme 2014-2018 under grant agreement No 633053. The views and opinions expressed herein do not necessarily reflect those of the European Commission.

[1] D.-G. Whyte, A. E. Hubbard, J. W. Hughes, B. Lipschultz, J. Rice, E. S. Marmar, M. Greenwald, I. Cziegler, A. Dominguez, T. Golfinopoulos, et al., Nucl. Fusion **50**, 105005 (2010).

[2] F. Ryter, S. W., B. Brüsehaber, M. Kaufmann, V. Mertens, H. Murmann, A. G. Peeters, J. Stober, J. Schweinzer, H. Zohm, et al., Plasma Phys. & Controlled Fusion **40**, 725 (1998).

[3] A. E. Hubbard, D. G. Whyte, R. M. Churchill, I. Cziegler, A. Dominguez, T. Golfinopoulos, J. W. Hughes, J. E. Rice, I. Bespamyatnov, M. J. Greenwald, et al., Phys. Plasmas **18**, 331 (2011).

[4] R. M. McDermott, B. Lipschultz, J. W. Hughes, P. J. Catto, A. E. Hubbard, I. H. Hutchinson, R. S. Granetz, M. Greenwald, B. LaBombard, K. Marr, et al., Phys. Plasmas **16**, 056103 (2009).

[5] I. Cziegler, P. H. Diamond, N. Fedorczak, P. Manz, G. R. Tynan, M. Xu, A. E. Hubbard, B. Lipschultz, J. M. Sierchio, J. L. Terry, et al., Phys. Plasmas **20**, 055904 (2013).

[6] A. E. Hubbard, T. Osborne, F. Ryter, M. Austin, L. Barrera Orte, R. M. Churchill, I. Cziegler, M. Fenstermacher, R. Fischer, S. Gerhardt, et al., Nucl. Fusion **56**, 086003 (2016).

[7] A. Hubbard et al., Proc. of the 26^{th} IAEA Fusion Energy Conf., Kyoto, Japan pp. EX3–1 (2016).

[8] F. Ryter, R. Fischer, J. C. Fuchs, T. Happel, R. M. McDermott, E. Viezzer, E. Wolfrum, L. Barrera Orte, M. Bernert, A. Burckhart, et al., Nucl. Fusion **57**, 016004 (2017).

[9] A. Marinoni, J. Rost, M. Porkolab, A. Hubbard, T. Osborne, A. White, D. Whyte, T. Rhodes, E. Davis, D. Ernst, et al., Nucl. Fusion **55**, 093019 (2015).

[10] T. Happel, P. Manz, F. Ryter, M. Bernert, M. Dunne, P. Hennequin, A. Hetzenecker, U. Stroth, G. D. Conway, L. Guimarais, et al., Plasma Phys. & Controlled Fusion **59**, 014004 (2017).

[11] Y. R. Martin, T. Takizuka, and the ITPA CDBM H-mode Threshold Database Working Group, J. Phys.: Conf. Ser. **123**, 012033 (2008).

[12] P. Manz, P. Lauber, V. E. Nikolaeva, T. Happel, F. Ryter, G. Birkenmeier, A. Bogomolov, G. D. Conway, M. E. Manso, M. Maraschek, et al., Nucl. Fusion **55**, 083004 (2015).

[13] T. Happel, P. Manz, F. Ryter, P. Hennequin, A. Hetzenecker, G. D. Conway, L. Guimarais, C. Honoré, U. Stroth, E. Viezzer, et al., Nucl. Fusion **56**, 064004 (2016).

[14] L. Cupido, S. Graca, G. D. Conway, M. Manso, F. Serra, and the ASDEX Upgrade Team, Rev. Sci. Inst. **77**, 10E915 (2006).

[15] Y. Nagashima, K. Itoh, S.-I. Itoh, A. Fujisawa, M. Yagi, K. Hoshino, S. Shinohara, A. Ejiri, Y. Takase, T. Ido, et al., Plasma Phys. & Controlled Fusion **49**, 1611 (2007).

[16] D. Prisiazhniuk, A. Krämer-Flecken, G. D. Conway, T. Happel, P. Manz, P. Simon, M. Dunne, U. Stroth, and the ASDEX Upgrade Team, 12th Int. Reflectometer Workshop (FZ Jülich, Germany (2015).

[17] Z. X. Liu, X. Q. Xu, X. Gao, A. E. Hubbard, J. W. Hughes, J. R. Walk, C. Theiler, T. Y. Xia, S. G. Baek, T. Golfinopoulos, et al., Phys. Plasmas **23**, 120703 (2016).

[18] P. Lauber, S. Günter, A. Könies, and S. D. Pinches, Journal Of Computational Physics **226**, 447 (2007).

[19] L. Villard and J. Vaclavik, Nucl. Fusion **37**, 351 (1997).

[20] F. Mink, E. Wolfrum, M. Maraschek, H. Zohm, L. Horvath, F. M. Laggner, P. Manz, E. Viezzer, U. Stroth, and the ASDEX Upgrade Team, Plasma Phys. & Controlled Fusion **58**, 125013 (2016).

[21] M. Cavedon, T. Puetterich, E. Viezzer, G. Birkenmeier, T. Happel, F. M. Laggner, P. Manz, F. Ryter, U. Stroth, and Asdex Upgrade Team, Nucl. Fusion **57**, 014002 (2017).

[22] G. Birkenmeier, M. Cavedon, G. D. Conway, P. Manz, G. Fuchert, F. M. Laggner, T. Happel, A. Medvedeva, V. Nikolaeva, D. Prisiazhniuk, et al., Nucl. Fusion **56**, 086009 (2016).

[23] V. V. Bulanin, V. I. Varfolomeev, V. K. Gusev, A. E. Ivanov, S. V. Krikunov, G. S. Kurskiev, M. M. Larionov, V. B. Minaev, M. I. Patrov, A. V. Petrov, et al., Technical Physics Letters **37**, 340 (2011).

[24] M. Bernert, T. Eich, A. Burkhart, J. C. Fuchs, L. Giannone, A. Kallenbach, R. M. McDermott, B. Sieglin, and the ASDEX Upgrade Team, Rev. Sci. Inst. **85**, 033503 (2014).

[25] T. Kobayashi, S. Inagaki, M. Sasaki, Y. Kosuga, H. Arakawa, T. Yamada, Y. Nagashima, Y. Miwa, N. Kasuya, A. Fujisawa, et al., Phys. Plasmas **22**, 112301 (2015).

[26] G. D. Conway, B. Scott, J. Schirmer, M. Reich, A. Kendl, and the ASDEX Upgrade Team, Plasma Phys. & Controlled Fusion **47**, 1165 (2005).

[27] A. Fujisawa et al., Plasma Phys. & Controlled Fusion **48**, S31 (2006).

[28] T. Ido et al., Nucl. Fusion **46**, 512 (2006).

[29] A. V. Melnikov, V. A. Vershkov, L. G. Eliseev, S. A. Grashin, A. V. Gudozhnik, L. I. Krupnik, S. E. Lysenko, V. A. Mavrin, S. V. Perfilov, D. A. Shelukhin, et al., Plasma Phys. & Controlled Fusion **48**, S87 (2006).

[30] Y. Hamada, T. Watari, A. Nishizawa, T. Ido, M. Kojima, Y. Kawasumi, K. Toi, and the JIPPT-IIU Group, Plasma Phys. & Controlled Fusion **48**, S177 (2006).

[31] J. Cheng, L. Yan, K. Zhao, J. Dong, W. Hong, J. Qian, Q. Yang, X. Ding, X. Duan, and Y. Liu, Nucl. Fusion **49**, 085030 (2009).

[32] J. R. Robinson, B. Hnat, P. Dura, A. Kirk, P. Tamain, and the MAST Team, Plasma Phys. & Controlled Fusion **54**, 105007 (2012).

[33] J. C. Hillesheim, W. A. Peebles, T. A. Carter, L. Schmitz, and T. L. Rhodes, Phys. Plasmas **19**, 022301 (2012).

[34] A. Storelli, L. Vermare, P. Hennequin, . D. Grcan, G. Dif-Pradalier, Y. Sarazin, X. Garbet, T. Grler, R. Singh, P. Morel, et al., Physics of Plasmas **22**, 062508 (2015).

[35] C. Silva, J. C. Hillesheim, C. Hidalgo, E. Belonohy, E. Delabie, L. Gil, C. F. Maggi, L. Meneses, E. Solano, M. Tsalas, et al., Nucl. Fusion **56**, 106026 (2016).

[36] V. Bulanin, V. Gusev, A. Iblyaminova, N. Khromov, G. Kurskiev, V. Minaev, M. Patrov, A. Petrov, Y. Petrov, N. Sakharov, et al., Nuclear Fusion **56**, 016017 (2016).

[37] A. D. Gurchenko, E. Z. Gusakov, P. Niskala, A. B. Altukhov, L. A. Esipov, T. P. Kiviniemi, T. Korpilo, D. V. Kouprienko, S. I. Lashkul, S. Leerink, et al., Plasma Phys. & Controlled Fusion **58**, 044002 (2016).

[38] V. V. Bulanin, L. G. Askinazi, A. A. Belokurov, V. A. Kornev, V. Lebedev, A. V. Petrov, A. S. Tukachinsky, M. I. Vildjunas, F. Wagner, and A. Y. Yashin, Plasma Phys. & Controlled Fusion **58**, 045006 (2016).

[39] K. Miki, Y. Y. Kishimoto, N. Miyato, and J. Q. Li, Phys. Rev. Lett. **99**, 145003 (2007).

[40] A. Tsinober, ed., *An informal introduction to turbulence* (Kluwer Academic Publishers, 2001, Dortrecht).

[41] T. Klinger, A. Latten, A. Piel, G. Bonhomme, and T. Pierre, Plasma Phys. & Controlled Fusion **39**, 1 (1997).

[42] M. J. Burin, G. R. Tynan, G. Y. Antar, N. A. Crocker, and C. Holland, Phys. Plasmas **12**, 052320 (2006).

[43] P. Manz, M. Xu, S. C. Thakur, and G. R. Tynan, Plasma Phys. & Controlled Fusion **53**, 095001 (2011).

[44] A. Diallo, J. W. Hughes, M. Greenwald, B. LaBombard, E. Davis, S.-G. Baek, C. Theiler, P. Snyder, J. Canik, J. Walk, et al., Phys. Rev. Lett. **112**, 115001 (2014).

[45] F. M. Laggner, E. Wolfrum, M. Cavedon, F. Mink, E. Viezzer, M. G. Dunne, P. Manz, H. Doerk, G. Birkenmeier, R. Fischer, et al., Plasma Phys. & Controlled Fusion **58**, 065005 (2016).

[46] B. P. van Milligen, C. Hidalgo, and E. Sanchez, Phys. Rev. Lett. **74**, 395 (1995).

[47] Y. Nagashima, K. Hoshino, A. Ejiri, K. Shinohara, Y. Takase, K. Tsuzuki, K. Uehara, H. Kawashima, H. Ogawa, T. Ido, et al., Phys. Rev. Lett. **95**, 095002 (2005).

[48] K. J. Zhao, T. Lan, J. Q. Dong, L. W. Yan, W. Y. Hong, C. X. Yu, A. D. Liu, J. Qian, J. Cheng, D. L. Yu, et al., Phys. Rev. Lett. **96**, 255004 (2006).

[49] P. H. Diamond, S. I. Itoh, and K. Itoh, eds., *Modern Plasma Physics* (Cambridge University Press, 2010, New York).

[50] P. Manz, M. Xu, N. Fedorczak, S. C. Thakur, and G. R. Tynan, Phys. Plasmas **19**, 012309 (2012).

[51] E. Balkovsky, G. Falkovich, I. Kolokolov, and L. V., Phys. Rev. Lett. **78**, 1452 (1997).

[52] A. Zeiler, J. F. Drake, and B. Rogers, Phys. Plasmas **4** (1997).

[53] A. E. White, P. Phillips, D. G. Whyte, A. E. Hubbard, C. Sung, J. W. Hughes, A. Dominguez, J. Terry, and I. Cziegler, Nucl. Fusion **51**, 113005 (2011).

[54] B. D. Scott, Phys. Plasmas **12**, 062314 (2005).

[55] M. Griener, O. Schmitz, K. Bald, D. Bsser, M. Cavedon, P. D. Marn, T. Eich, G. Fuchert, A. Herrmann, A. Kappatou, et al., Review of Scientific Instruments **88**, 033509 (2017).

[56] S. J. Freethy, G. D. Conway, I. Classen, A. J. Creely, T. Happel, A. Khn, B. Vanovac, and A. E. White, Review of Scientific Instruments **87**, 11E102 (2016).